AIAA JOURNAL
Vol. 33, No. 11, November 1995

Multigrid Algorithm for Three-Dimensional Incompressible High-Reynolds Number Turbulent Flows

Chunhua Sheng,* Lafayette K. Taylor,† and David L. Whitfield‡
Mississippi State University, Mississippi State, Mississippi 39762

In this paper, a robust multigrid algorithm is presented for solving three-dimensional incompressible high-Reynolds number turbulent flows on high aspect ratio grids. The artificial compressibility form of the Navier–Stokes equations is discretized in a cell-centered finite volume form on a time-dependent curvilinear coordinate system, and the so-called discretized Newton-relaxation scheme is used as the iterative procedure for the solution of the system of equations. A nonlinear multigrid scheme (full approximation scheme [FAS]) is applied to accelerate the convergence of the time-dependent equations to a steady state. Two methods for constructing the coarse grid operator, the Galerkin coarse grid approximation and the discrete coarse grid approximation have also been investigated and incorporated into the FAS. A new procedure, called implicit correction smoothing that leads to high efficiency of the multigrid scheme by allowing large Courant–Friedrichs–Lewy numbers, is introduced in this work. Numerical solutions of high-Reynolds number turbulent flows for practical engineering problems are presented to illustrate the efficiency and accuracy of the current multigrid algorithm.

I. Introduction

A RECENT trend in computational fluid dynamics (CFD) applications is to predict realistic engineering problems by solving the Navier–Stokes equations with high-resolution schemes.[1,2] Numerical simulations of three-dimensional high-Reynolds number turbulent flows, however, require a very large number of grid points and extremely small grid spacing in order to fully resolve the turbulent boundary layer and to obtain a grid independent solution. As in most iterative methods that are used in existing solution algorithms, the convergence rate slows down rapidly when the system gets larger and grids become more stretched. In addition, a very small grid spacing may cause extremely high aspect ratio cells for turbulent flow grids, which is one of the major obstacles for many codes to simulate realistic flows due to numerical instability.[1] For this reason, these codes are unable to simulate very high-Reynolds number flows, such as $Re = 10^9$, without using wall functions. To make Navier–Stokes solutions useful as a design tool in engineering, substantial improvement in efficiency of existing solution techniques has to be made.

Among acceleration techniques, the multigrid method is said to be the most efficient and general acceleration technique known today.[3] Numerous references can be found on this topic.[4–6] The advantage of the multigrid method over other acceleration techniques is the fact that under quite general circumstances, where the relaxation scheme has a good damping rate for the entire spectrum, the rate of convergence is independent of the size of the system to be solved.[6] This makes the multigrid method especially useful and suitable for the solution of turbulent flows where very fine discretization is needed.

In this work, a nonlinear full approximation scheme (FAS)[3] is used to accelerate the convergence of an implicit high-resolution scheme[7] in highly stretched grids for high-Reynolds number turbulent flows. A simple way to construct the coarse grid operator, the Galerkin coarse grid approximation (GCA), is developed in this work. A new procedure, called implicit correction smoothing, is incorporated into the multigrid scheme. This new procedure plays an important role in the current algorithm.

In the following, a brief description is given of the three-dimensional incompressible Navier–Stokes equations based on the artificial compressibility idea of Chorin,[8] the finite volume discretization using the Roe[9] flux formulation to evaluate the numerical flux at cell faces, and the numerical method for solving the system of equations, which is referred to as discretized Newton-relaxation (DNR) in Ref. 10. In Sec. III, the nonlinear multigrid algorithm FAS is described. Comparisons are made between the GCA and the discrete coarse grid approximation (DCA) and semicoarsening and full-coarsening strategies on the efficiency of multigrid solutions. In Sec. IV, numerical solutions are presented for turbulent flows about the SUBOFF bare hull configuration[11] at a Reynolds number of 1.2×10^7 and 1.2×10^9, and for flow about a 6:1 prolate spheroid[12] at 10-deg angle of attack. The study of the grid sensitivity of the current multigrid algorithm to grid spacings is also carried out. All solutions were obtained on a single processor workstation IBM RS6000/560. In the last section some conclusions are summarized.

II. Basic Flow Solver

Governing Equations

The artificial compressibility form of the three-dimensional incompressible time-dependent Navier–Stokes equations in general curvilinear coordinates is

$$\frac{\partial Q}{\partial \tau} + \frac{\partial F}{\partial \xi} + \frac{\partial G}{\partial \eta} + \frac{\partial H}{\partial \zeta} = 0 \tag{1}$$

where

$$Q = J \begin{bmatrix} p \\ u \\ v \\ w \end{bmatrix} \qquad K = J \begin{bmatrix} \beta(\theta_k - k_t) \\ u\theta_k + k_x p - \tilde{T}_{k_x} \\ v\theta_k + k_y p - \tilde{T}_{k_y} \\ w\theta_k + k_z p - \tilde{T}_{k_z} \end{bmatrix}$$

and

$$\theta_k = k_t + k_x u + k_y v + k_z w$$

$$K = F, \quad \theta_k = U \quad \text{for} \quad k = \xi$$

$$K = G, \quad \theta_k = V \quad \text{for} \quad k = \eta$$

$$K = H, \quad \theta_k = W \quad \text{for} \quad k = \zeta$$

In the preceding equations, β is the artificial compressibility coefficient, with a typical value of $5 \sim 10$; p is static pressure; u, v, and w are the velocity components in Cartesian coordinates x, y,

Presented as Paper 94-2335 at the AIAA 25th Fluid Dynamics Conference, Colorado Springs, CO, June 20–23, 1994; received Jan. 9, 1995; revision received May 10, 1995; accepted for publication May 22, 1995.

*Postdoctoral Fellow, Computational Fluid Dynamics Laboratory, NSF Engineering Research Center. Member AIAA.

†Research Engineer, Computational Fluid Dynamics Laboratory, NSF Engineering Research Center. Member AIAA.

‡Professor, Department of Aerospace Engineering, Computational Fluid Dynamics Laboratory, NSF Engineering Research Center. Member AIAA.

and z. U, V, and W are the contravariant velocity components in curvilinear coordinate directions ξ, η, and ζ, respectively. Terms $\tilde{T}_{k_x}$, $\tilde{T}_{k_y}$, $\tilde{T}_{k_z}$, where $k = \xi, \eta$, and ζ, are the viscous flux components in curvilinear coordinates. J is the Jacobian of the inverse transformation, and k_x, k_y, k_z, and k_t with $k = \xi, \eta$, and ζ are the transformation metric quantities. Evaluations of these quantities are well known and are not repeated here.

In this work, the thin-layer approximation is introduced to simplify the full Navier–Stokes equations, and a Baldwin–Lomax algebraic turbulence model is adopted for turbulent flow computations.

Numerical Flux Evaluation

The Navier–Stokes equations (1) are discretized by an implicit cell-centered finite-volume scheme. In the one-dimensional case, it may be written as

$$\left[\left(Q_i^{n+1} - Q_i^n\right)/\Delta\tau\right] + \left(\bar{F}_{i+\frac{1}{2}}^{n+1} - \bar{F}_{i-\frac{1}{2}}^{n+1}\right) = 0 \tag{2}$$

where the index i corresponds to a cell center and indices $i \pm \frac{1}{2}$ correspond to cell faces. In this expression, the dependent variable vector Q is considered to be constant throughout the cell whereas the flux $\bar{F}$ is assumed to be uniform over each surface of the cell. Clearly, this finite volume discretization requires the evaluation of the flux vector $\bar{F}$ at cell faces.

There are numerous ways of obtaining the flux vector $\bar{F}$ at cell faces; however, the quality of the numerical solution is critically dependent on how the flux vector is formulated. Numerous ways of forming the flux vector have been investigated in Ref. 13, and it was found that the Roe[9] scheme, which is within the class of a Godunov-type approach, provides computational efficiency and an accurate method to obtain the numerical flux. The numerical flux of a higher order Roe scheme using total variation diminishing (TVD) limiting has been introduced by Osher and Chakravarthy[14]; however, it is found that TVD limiting has thus far not been required for incompressible flows. Following Ref. 15, the numerical flux of a higher order scheme without using TVD limiting is

$$\begin{aligned}\bar{F}_{i+\frac{1}{2}} &= [F(Q_i)]_{i+\frac{1}{2}} + \sum_{j=1}^{n} \sigma^-_{j,i+\frac{1}{2}} r^{(j)}_{i+\frac{1}{2}} \\ &+ \sum_{j=1}^{n} \left\{ \frac{1-\psi}{4}\left[\sigma^+_{j,i-\frac{1}{2}} - \sigma^-_{j,i+\frac{3}{2}}\right] \right. \\ &\left. + \frac{1+\psi}{4}\left[\sigma^+_{j,i+\frac{1}{2}} - \sigma^-_{j,i+\frac{1}{2}}\right] \right\} r^{(j)}_{i+\frac{1}{2}}\end{aligned} \tag{3}$$

where the σ_j used in Eq. (3) are defined as

$$\sigma^{\pm}_{j,i+p/2} = \lambda^{\pm(j)}_{i+\frac{1}{2}} \alpha_{j,i+p/2}$$

$$\alpha_{j,i-\frac{1}{2}} = l^{(j)}_{i+\frac{1}{2}} \cdot (Q_i - Q_{i-1})$$

$$\alpha_{j,i+\frac{1}{2}} = l^{(j)}_{i+\frac{1}{2}} \cdot (Q_{i+1} - Q_i)$$

$$\alpha_{j,i+\frac{3}{2}} = l^{(j)}_{i+\frac{1}{2}} \cdot (Q_{i+2} - Q_{i+1})$$

In the preceding expressions, $\lambda^{\pm}$ correspond to the positive and negative eigenvalues of the Roe matrix, respectively, and $r^{(j)}$ and $l^{(j)}$ correspond to the right and left eigenvectors of the Roe matrix. With $\psi = -1$ a second-order scheme results. With $\psi = \frac{1}{3}$ a third-order upwind-biased scheme results. In this work, a third-order Roe flux scheme is used for all of the computations.

Numerical Solution Method

Since the discretized Eq. (2) is nonlinear, Newton's method described in Ref. 7 is used to linearize the equation. Note that Eq. (2) can be written in a simple form as

$$N(Q^{n+1}) = 0 \tag{4}$$

Applying Newton's method to Eq. (4) yields

$$N'(Q^{n+1,m})(Q^{n+1,m+1} - Q^{n+1,m}) = -N(Q^{n+1,m}) \tag{5}$$

where $m = 1, 2, 3, \ldots$, and $N'(Q^{n+1,m})$ is the Jacobian matrix of the vector $N(Q^{n+1})$. The resulting formulation of Eq. (2) is

$$\begin{aligned}&-\bar{F}'_{i-\frac{1}{2},i-1}\Delta Q_{i-1}^{n+1,m} \\ &+ \bar{F}'_{i+\frac{1}{2},i+1}\Delta Q_{i+1}^{n+1,m} + \left(\frac{I}{\Delta\tau} + \bar{F}'_{i+\frac{1}{2},i} - \bar{F}'_{i-\frac{1}{2},i}\right)\Delta Q_i^{n+1,m} \\ &= -\left[I_a \frac{Q_i^{n+1,m} - Q_i^n}{\Delta\tau} + \left(\bar{F}_{i+\frac{1}{2}}(Q^{n+1,m}) - \bar{F}_{i-\frac{1}{2}}(Q^{n+1,m})\right)\right]\end{aligned} \tag{6}$$

In this expression, $\bar{F}'$ is the Jacobian of the numerical flux vector, with the first subscript representing the position of the cell face of the numerical flux vector and the second subscript representing the position of the dependent variable vector that the numerical flux vector is differentiated with respect to. I_a is an identity matrix, except the first diagonal element is zero in order to satisfy the true incompressible continuity equation. Note that at the first Newton iteration $Q^{n+1,1} = Q^n$.

A direct solution of this linear system of equations, which must be solved at each iteration of Newton's method, is not feasible for general three-dimensional problems. In practice, one rather seeks variations or approximations of Newton's method, such as a factorization scheme or a relaxation scheme. In this work, a symmetric Gauss–Seidel relaxation has been chosen as an approximation to Newton's method, which is referred to as Newton-relaxation, with Newton being the primary iteration and relaxation the secondary iteration. Since the flux Jacobians $\bar{F}'$ in Eq. (6) are evaluated by the discretized numerical derivative, this whole procedure is called DNR.[7,10]

III. Multigrid Algorithm

Nonlinear Full Approximation Scheme

In order to solve Eq. (2) or (4) with the multigrid method, a hierarchy of grids is defined and indicated by a level $L = \{h, 2h, 4h, \ldots,\}$ where lh, $l = 1, 2, 4, \ldots$, denotes the grid on the finest mesh to successively coarser meshes that are formed by eliminating every other grid line on the previous finer mesh. The multigrid strategy used in this work is a standard nonlinear FAS V-cycle.[3] Consider a general nonlinear equation

$$N(\boldsymbol{Q}) = f \tag{7}$$

where $\boldsymbol{Q}$ is the exact solution, and the source term f is zero on the finest grid for the Navier–Stokes equations. One FAS V-cycle for Eq. (7) consists of the following steps.

Step 1 (prerelaxation): Start with an initial guess Q_0^h on the finest grid h. Iterate the equation $N^h(Q^h) = f^h v_1$ times to obtain an approximate solution Q^h.

Step 2 (coarse grid solution): If the present grid is the coarsest, go to step 3. Otherwise, calculate the residual

$$r^h = f^h - N^h(Q^h) \tag{8}$$

on the current grid. Restrict the residual r^h and the solution Q^h to the next coarser grid $2h$ by

$$r^{2h} = R_h^{2h} r^h \qquad Q_0^{2h} = I_h^{2h} Q^h \tag{9}$$

where R_h^{2h} and I_h^{2h} are two restriction operators. Calculate the right-hand side of Eq. (7) on the coarse grid $2h$ by

$$f^{2h} = N^{2h}\left(Q_0^{2h}\right) + r^{2h} \tag{10}$$

and iterate the equation $N^{2h}(Q^{2h}) = f^{2h}$ on grid $2h$ (using Q_0^{2h} as the initial guess) to obtain an approximate solution Q^{2h}. Repeat this step until the coarsest grid is reached.

Step 3 (coarse grid correction): Interpolate the coarse grid correction ΔQ^{2h} to the previous finer grid h and update the solution Q^h

$$\Delta Q^h = P_{2h}^h \Delta Q^{2h} \qquad Q^h \leftarrow Q^h + \Delta Q^h \tag{11}$$

where P_{2h}^h is the prolongation operator. An implicit correction smoothing (discussed later) is applied to ΔQ^h before updating the solution Q^h.

Step 4 (postrelaxation): Use Q^h as an initial guess and iterate the equation $N^h(Q^h) = f^h v_2$ times on grid h to obtain an approximate solution. Repeat steps 3 and 4 until the finest grid is reached.

Another multigrid strategy, W-cycle, may be implemented by applying two V-cycles on each coarse grid recursively. In this work, the V-cycle is used with one prerelaxation ($v_1 = 1$) and without postrelaxation ($v_2 = 0$) on each grid level during a multigrid cycle. To complete the description of the FAS cycle, one needs to be explicit about the relaxation method for the nonlinear system of equations and the choice of restriction operators R_h^{2h} and I_h^{2h}, prolongation operator P_{2h}^h, and coarse grid operator N^{2h}. These will be described next.

Nonlinear Relaxation Method

Recall that when the FAS scheme is applied to Eq. (7), the resulting formulation on any coarse grid level $2h$ can be written as

$$N^{2h}(Q^{2h}) = f^{2h} = R_h^{2h} f^h + \tau^{2h} \tag{12}$$

where

$$\tau^{2h} = N^{2h}\left(Q_0^{2h}\right) - R_h^{2h} N^h(Q^h)$$

is the defect correction (or relative truncation error between the coarse grid $2h$ and the previous finer grid h), and $\tau^h = 0$ on the finest grid. The DNR method mentioned before is used as a smoother to the multigrid scheme. Thus, applying the Newton's method to the coarse grid Eq. (12) yields

$$N'^{2h}(Q^{2h})\Delta Q^{2h} = -[N^{2h}(Q^{2h}) - f^{2h}]$$

or

$$N'^{2h}(Q^{2h})\Delta Q^{2h} = -\left[N^{2h}(Q^{2h}) - N^{2h}\left(I_h^{2h} Q^h\right) - R_h^{2h}(f^h - N^h(Q^h))\right] \tag{13}$$

Notice that in the first step of the Newton iteration, the term $N^{2h}(Q^{2h})$ cancels $N^{2h}(I_h^{2h} Q^h)$, and Eq. (13) is equivalent to solving

$$N'^{2h}(Q^{2h})\Delta Q^{2h} = R_h^{2h}(f^h - N^h(Q^h)) = r^{2h} \tag{14}$$

The resulting formulation of Eq. (2) by a one-step Newton's method is

$$-\bar{F}'^{2h}_{i-\frac{1}{2},i-1}\Delta Q^{2h}_{i-1} + \bar{F}'^{2h}_{i+\frac{1}{2},i+1}\Delta Q^{2h}_{i+1} + \left(\frac{1}{\Delta\tau} + \bar{F}'^{2h}_{i+\frac{1}{2},i} - \bar{F}'^{2h}_{i-\frac{1}{2},i}\right)\Delta Q_i^{2h} = r_i^{2h} \tag{15}$$

Comparing with Eq. (6), the right-hand side of Eq. (15) on any coarse grid $2h$ is the restriction of the residual of Eq. (12) on the previous finer grid h. Equation (15) is a linear system and is solved approximately by symmetric Gauss–Seidel relaxations.

Restriction, Prolongation, and Coarse Grid Operators

To be consistent with the concept of a finite volume discretization, natural and cost-effective restriction and prolongation operators are selected as follows: to use summation over the subcells that form a coarse grid cell for R_h^{2h} and to use a piecewise constant interpolation for P_{2h}^h (Ref. 16). That is,

$$\left(R_h^{2h} r^h\right)_{I,J,K} = \sum_{i,j,k} r_{i,j,k}^h \tag{16}$$

$$\left(P_{2h}^h \Delta Q^{2h}\right)_{i,j,k} = \Delta Q_{I,J,K}^{2h} \tag{17}$$

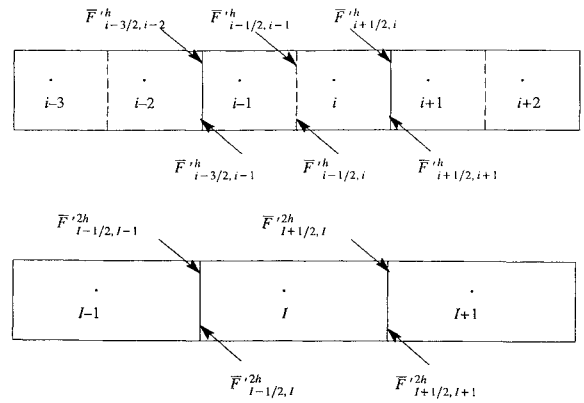

Fig. 1 Fine grid and coarse grid cells.

where indices i, j, and k denote a fine grid cell and I, J, and K denote a coarse grid cell. Another interpolation based on the volume averaging for prolongation operator P_{2h}^h has also been tried, but no significant change on convergence was found in the test problems. The real benefit of piecewise constant interpolation is that the coarse grid operator is easily constructed using the Galerkin approximation method, as described next. The dependent variables that are transferred from the fine grid to the coarse grid are obtained by a volume averaging:

$$\left(I_h^{2h} Q^h\right)_{I,J,K} = \sum_{i,j,k} \mathrm{vol}_{i,j,k}^h Q_{i,j,k}^h \Big/ \sum_{i,j,k} \mathrm{vol}_{i,j,k}^h \tag{18}$$

For the coarse grid operator N^{2h}, two approaches have been examined: discrete coarse grid approximation (DCA) and GCA. The first method means that the coarse grid operator N^{2h} is discretized directly from N on the coarse grid, analogous to the fine grid operator N^h. The second approach means that the coarse grid operator N^{2h} is constructed by the following formula[3]:

$$N^{2h} = R_h^{2h} N^h P_{2h}^h \tag{19}$$

In the following, the Galerkin approximation for the coarse grid operator will be derived. Consider the case of Eq. (15) with one Newton iteration applied to each time step. Let the subscript i denote the cell location on the current fine grid h and I denote the cell location on the next coarser grid $2h$. Applying the restriction operator R_h^{2h} to Eq. (15) [taking the summation of Eq. (15) at the fine grid cells $i-1$ and i that make up a coarse grid cell I (see Fig. 1)] yields

$$\begin{aligned} &-\bar{F}'^{h}_{i-\frac{3}{2},i-2}\Delta Q^h_{i-2} + \bar{F}'^{h}_{i-\frac{1}{2},i}\Delta Q^h_i \\ &+\left(\frac{I}{\Delta\tau^h_{i-1}} + \bar{F}'^{h}_{i-\frac{1}{2},i-1} - \bar{F}'^{h}_{i-\frac{3}{2},i-1}\right)\Delta Q^h_{i-1} \\ &-\bar{F}'^{h}_{i-\frac{1}{2},i-1}\Delta Q^h_{i-1} + \bar{F}'^{h}_{i+\frac{1}{2},i+1}\Delta Q^h_{i+1} \\ &+\left(\frac{I}{\Delta\tau^h_i} + \bar{F}'^{h}_{i+\frac{1}{2},i} - \bar{F}'^{h}_{i-\frac{1}{2},i}\right)\Delta Q^h_i = \left(r^h_{i-1} + r^h_i\right) \end{aligned} \tag{20}$$

Noting that with the restriction and prolongation operators just defined, one has $\Delta Q^{2h}_{I-1} = \Delta Q^h_{i-2}$, $\Delta Q^{2h}_I = \Delta Q^h_{i-1}$, $\Delta Q^{2h}_I = \Delta Q^h_i$, $\Delta Q^{2h}_{I+1} = \Delta Q^h_{i+1}$, and $r^{2h}_I = r^h_{i-1} + r^h_i$. Substituting these relations into Eq. (20) yields

$$-\bar{F}'^{2h}_{I-\frac{1}{2},I-1}\Delta Q^{2h}_{I-1} + \bar{F}'^{2h}_{I+\frac{1}{2},I+1}\Delta Q^{2h}_{I+1} + \left(\frac{I}{\Delta\tau^{2h}_I} + \bar{F}'^{2h}_{I+\frac{1}{2},I} - \bar{F}'^{2h}_{I-\frac{1}{2},I}\right)\Delta Q^{2h}_I = r^{2h}_I \tag{21}$$

where

$$\bar{F}'^{2h}_{I-\frac{1}{2},I-1} = \bar{F}'^{h}_{i-\frac{3}{2},i-2} \qquad \bar{F}'^{2h}_{I-\frac{1}{2},I} = \bar{F}'^{h}_{i-\frac{3}{2},i-1}$$

$$\bar{F}'^{2h}_{I+\frac{1}{2},I} = \bar{F}'^{h}_{i+\frac{1}{2},i} \qquad \bar{F}'^{2h}_{I+\frac{1}{2},I+1} = \bar{F}'^{h}_{i+\frac{1}{2},i+1}$$

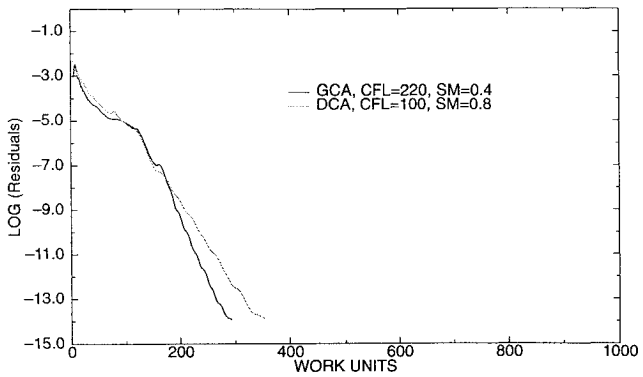

Fig. 2 Comparison of convergence rates of multigrid solutions with GCA and DCA.

For the three-dimensional case, the formulas should be updated as

$$\bar{F}^{\prime 2h}_{I-\frac{1}{2},I-1} = \sum_{j,k} \bar{F}^{\prime h}_{i-\frac{3}{2},i-2} \qquad \bar{F}^{\prime 2h}_{I-\frac{1}{2},I} = \sum_{j,k} \bar{F}^{\prime h}_{i-\frac{3}{2},i-1}$$
$$\bar{F}^{\prime 2h}_{I+\frac{1}{2},I} = \sum_{j,k} \bar{F}^{\prime h}_{i+\frac{1}{2},i} \qquad \bar{F}^{\prime 2h}_{I+\frac{1}{2},I+1} = \sum_{j,k} \bar{F}^{\prime h}_{i+\frac{1}{2},i+1} \tag{22}$$

From the derivation, the Jacobian of the flux vector at a coarse grid cell face can be obtained by taking the summation of Jacobians of the flux vector at previous finer grid cell faces that comprise the coarse grid cell face. The construction of the coarse grid operator only involves algebraic manipulations, avoiding the evaluation of Jacobians of flux vectors on the coarse grids that would be needed for the discrete approximation method. The local time step $\Delta\tau_I^{2h}$ in Eq. (21) is recalculated at each grid level. Numerical tests on both the GCA and DCA methods for the solution of SUBOFF bare hull[11] show that the two methods take nearly the same amount of work in constructing the coarse grid operators. The stability of the multigrid scheme, however, is different with respect to the two approaches. The maximum CFL number that could be used in the multigrid scheme with the GCA is higher than that with the DCA (Fig. 2). Although Eq. (22) is derived for one Newton iteration, it is still valid in the case of multiple Newton iterations implemented at each time step. Numerical tests show that more Newton iterations may be helpful to the convergence of the multigrid solution, however, the CPU time was found to be increased significantly. For this reason, only one Newton iteration, with five Gauss–Seidel relaxations, is implemented at each time step for all of the computations in this work.

Implicit Correction Smoothing

The idea of implicit correction smoothing has its origin in implicit residual smoothing, which was used by Jameson[4] in his explicit multigrid scheme. The difference between correction smoothing and residual smoothing is the time at which the smoothing process is made. In the former, the smoothing process is made on corrections after they are transferred from the next coarser grid but before they are used to update solutions on the finer grid. In the latter, however, the smoothing process takes place on residuals after they are collected from the previous finer grid and before being used for the relaxation. The implicit correction smoothing formula, analogous to residual smoothing,[4] can be written as

$$\left(1-\varepsilon_\xi\delta_\xi^2\right)\left(1-\varepsilon_\eta\delta_\eta^2\right)\left(1-\varepsilon_\zeta\delta_\zeta^2\right)\Delta Q^* = \Delta Q \tag{23}$$

where ΔQ and ΔQ^* are corrections to dependent variables before and after smoothing, and ε_ξ, ε_η and ε_ζ are the smoothing parameters in the ξ, η, and ζ directions. Values of ε_ξ, ε_η, and ε_ζ of about $0.4 \sim 0.8$ are considered to be nearly optimal through experiments.

As mentioned before, this work does not use postrelaxation during the multigrid cycle. Instead, implicit correction smoothing is used as a substitute for postrelaxation to eliminate the error introduced by interpolating the correction from the coarse grid to the finer grid. The reason for this choice is that the postrelaxation will greatly increase the computational work in each multigrid cycle, whereas implicit correction smoothing is much cheaper to implement. Another advantage of this technique is that the stability of the multigrid scheme may be improved so that a larger CFL number can be used. In general, after using an implicit correction smoothing and the values just suggested, the CFL number may be raised to at least two times the original value.

Semicoarsening and Full Coarsening

Deterioration of the convergence rate was encountered in some three-dimensional multigrid solutions when full coarsening was used. The same problems have been reported by Rosenfeld and Kwak.[17] This usually indicates a poor relaxation scheme or an inadequate coarsening method. One may either change the relaxation scheme by using block relaxations (such as plane Gauss–Seidel instead of point Gauss–Seidel), or applying a suitable semicoarsening strategy, i.e., doing coarsening only for certain coordinates. The first choice, however, complicates the solution algorithm, and therefore is inconvenient in practice. It was suggested by Brandt[3] that semicoarsening may be preferable for three-dimensional solutions and may serve as a general way to avoid the need of block relaxation. Numerical tests show that semicoarsening, when chosen properly, always provides better performance than full coarsening for the cases considered in this work. An example is given later.

IV. Results

SUBOFF Bare Hull

The first case considered is turbulent flow about the SUBOFF bare hull[11] at 0-deg angle of attack. The Reynolds number is 1.2×10^7 based on body length. Since the Reynolds number is very high, grid lines near the surface must be very dense in order to resolve the boundary layer. Three O-type grids, indicated by grid I, II, and III, were built with the same grid size ($129 \times 65 \times 2$), but different grid spacings near the surface (normal distance $\Delta = 1.0 \times 10^{-5}$, 1.0×10^{-6}, and 1.0×10^{-7}, based on the body length, with an average y^+ value of 3.67, 0.363, and 0.036, respectively), which results in extremely high aspect ratios of grid cells on the surface (Fig. 3). The purpose of this study is to investigate the grid sensitivity of the current multigrid scheme and to examine the efficiency and accuracy of the solution on such high aspect ratio and stretched grids, which are essential for simulation of high-Reynolds number turbulent flows. A five-level V-cycle multigrid with semicoarsening in the ξ and η directions was used for all of the grids. The flux Jacobians on the coarse grids were constructed using the GCA. Figure 4 shows the convergence histories of both the multigrid and single-grid solutions on three different grids at the listed Reynolds number, where both multigrid and single-grid solutions adopted the best possible CFL numbers. Very fast convergence rates were obtained in the multigrid solutions for all cases. The residuals are reduced to machine accuracy within 150–250 multigrid cycles, resulting in an effective radius of convergence from 0.913 to 0.945, which is a $45 \sim 60\%$ savings in CPU time over single-grid solutions. It should be pointed out that the CFL numbers for the multigrid solutions can be increased from initial values of $80 \sim 100$ to $180 \sim 220$ by using implicit correction smoothing. This increase in CFL numbers significantly improves the convergence rate.

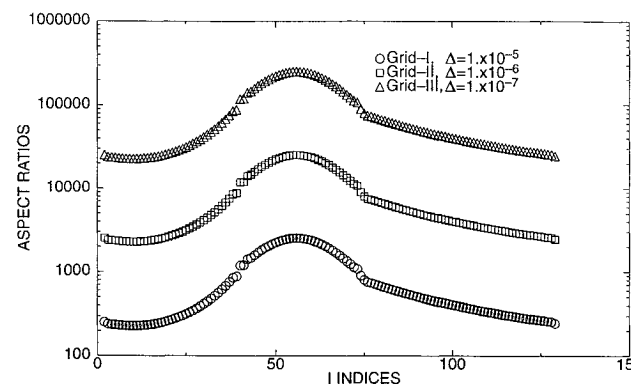

Fig. 3 Aspect ratios of first cells near surface of three SUBOFF bare hull grids.

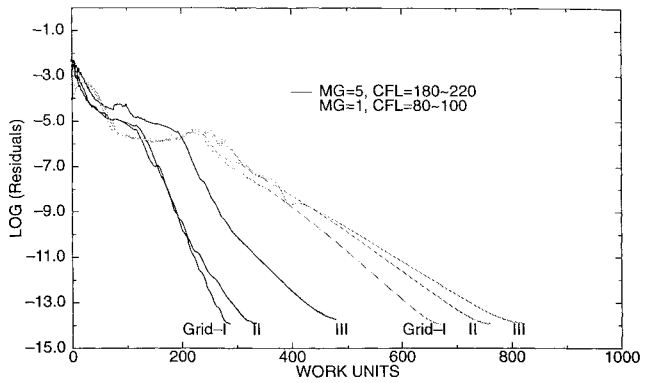

Fig. 4 Convergence histories of multigrid and single-grid solutions on three SUBOFF bare hull grids at $Re = 1.2 \times 10^7$.

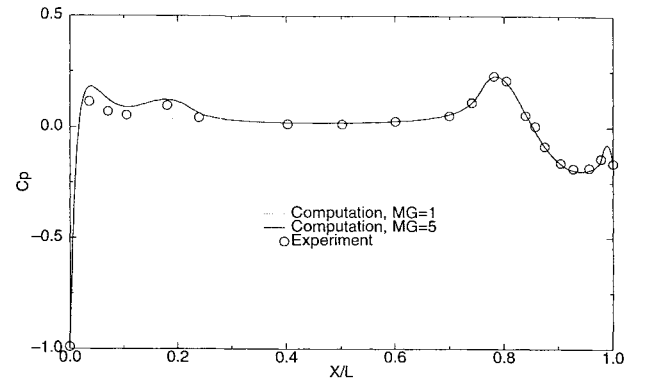

Fig. 5 C_p distributions on the SUBOFF hull surface at $Re = 1.2 \times 10^7$.

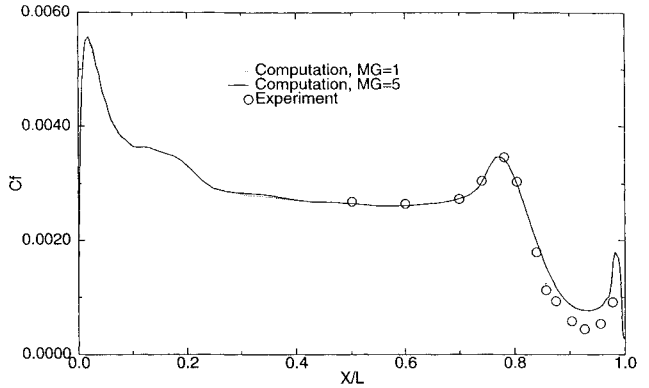

Fig. 6 C_f distributions on the SUBOFF hull surface at $Re = 1.2 \times 10^7$.

Figure 4 also shows that the convergence property of the multigrid scheme is not sensitive to the grid spacing for up to 1.0×10^{-6} of the body length ($y^+ = 0.363$), and the current code turns out to be robust in handling extremely high aspect ratio grids, although the value of y^+ of about 1 is adequate for resolving the viscous flows near the surface and for obtaining grid-independent solutions. The convergence rate is a little bit slower on the third grid (with spacing $\Delta = 1.0 \times 10^{-7}$) than the previous two grids but is still quite satisfactory. The smoothing parameter in the third grid needs to be increased to 0.8 (0.4 on the other two grids) to maintain stability of the multigrid solution at such a CFL number.

The surface pressure coefficient C_p and skin friction coefficient C_f are shown in Figs. 5 and 6, respectively, based on the third grid solution ($\Delta = 1.0 \times 10^{-7}$). They match reasonably well with the experimental data,[11] and little difference can be found between the multigrid and single-grid solutions.

An interesting phenomenon about skin friction C_f is that the final solution of the multigrid scheme is reached at an earlier stage of the residual level than the single-grid scheme; see Fig. 7. The C_f curve does not change for the multigrid solution after the residual is dropped nearly 3 orders of magnitude from the initial −2.37

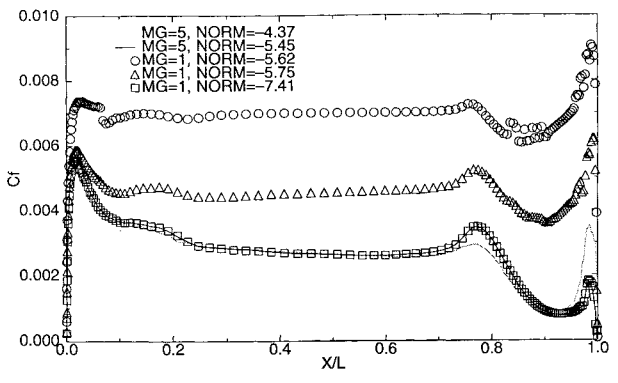

Fig. 7 Computed C_f distributions at different residual levels.

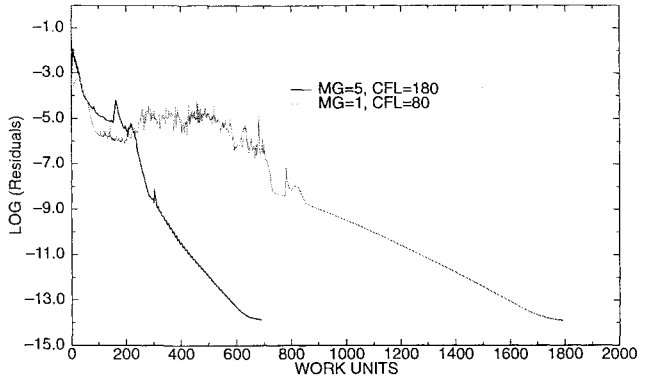

Fig. 8 Convergence histories of multigrid and single-grid solutions about SUBOFF bare hull at $Re = 1.2 \times 10^9$.

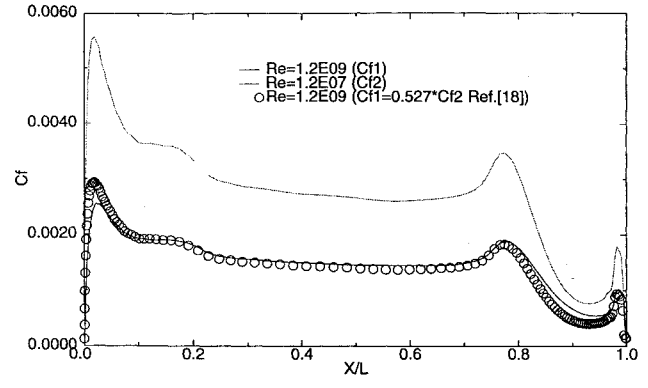

Fig. 9 Comparison of C_f distributions on SUBOFF hull surface at $Re = 1.2 \times 10^7$ and $Re = 1.2 \times 10^9$.

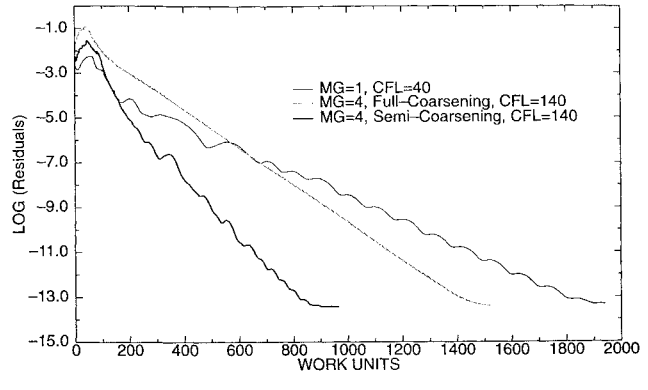

Fig. 10 Convergence histories of multigrid and single-grid solutions about 6:1 prolate spheroid at $Re = 4.2 \times 10^6$.

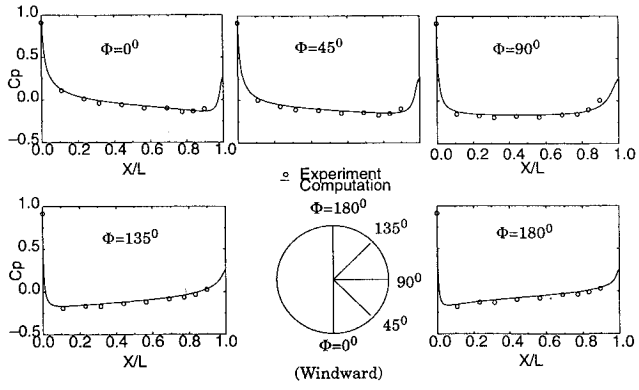

Fig. 11 Computed and measured C_p distributions on 6:1 prolate spheroid at α = 10 deg.

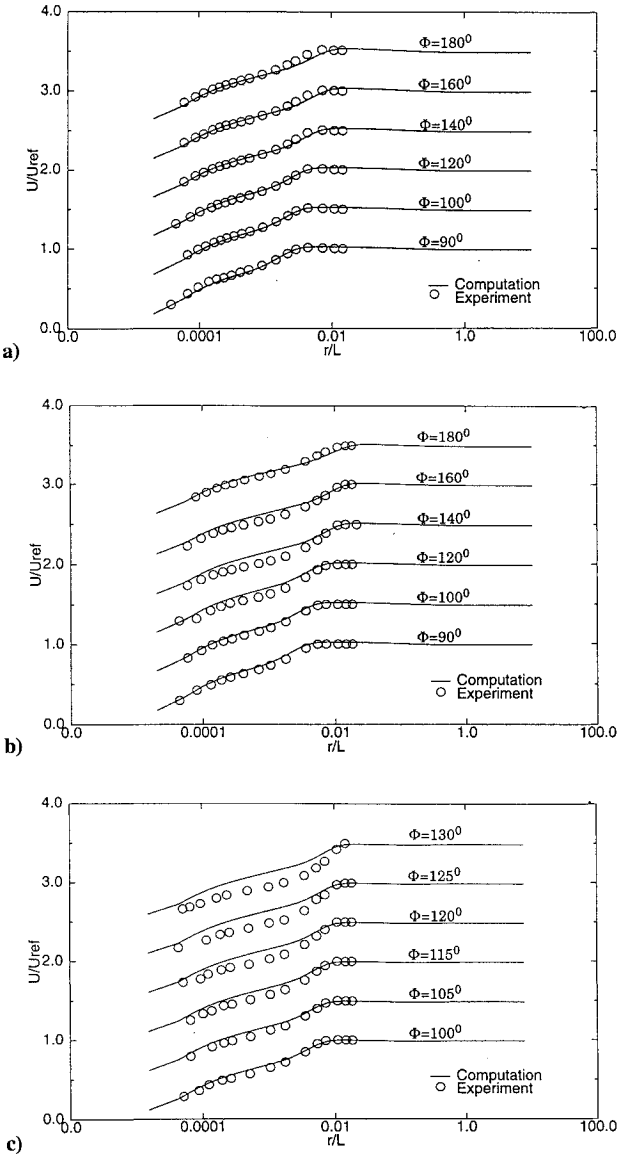

Fig. 12 Computed and measured U-velocity profiles at a) X/L = 0.4, b) X/L = 0.6, and c) X/L = 0.772.

to −5.11. But for the single-grid solution, a reduction of 5 orders of magnitude in residual (from initial −2.37 to −7.41) is required to reach the final solution. The implication of this result is that the actual savings in CPU time of the multigrid solution over the single grid should be higher than the figures just given.

A solution at a very high-Reynolds number, $Re = 1.2 \times 10^9$, was obtained on the third grid with the grid spacing $\Delta = 1.0 \times 10^{-7}$, which resulted in the average y^+ value being 2.62 of the first grid line near the surface. This y^+ value is small enough to resolve the viscous sublayer at this high-Reynolds number. The convergence histories of both the multigrid and single-grid solutions are shown in Fig. 8. Although the convergence rates of both multigrid and single-grid solutions at this Reynolds number are slower than those at the previous Reynolds number, a 65% savings in CPU time is still achieved with the multigrid solution over the single-grid solution. Since no experimental data are available at such a high-Reynolds number, a correlative comparison is made on the C_f curve at $Re = 1.2 \times 10^7$ and $Re = 1.2 \times 10^9$ using the formula given in Ref. 18; see Fig. 9. It seems that a reasonable skin friction is obtained at this Reynolds number.

Ratio 6:1 Prolate Spheroid at 10-deg Angle of Attack

A second test case was performed on a 6:1 prolate spheroid at 10-deg angle of attack.[12] The Reynolds number is 4.2×10^6 based on the model length and the freestream velocity. Since this is a fully three-dimensional flow, a half-physical space of the flowfield was solved using an O-type grid with a size of $81 \times 41 \times 41$. The average y^+ of the first grid line near the body was 2.56. Numerical solutions were obtained for the single grid and the four-level multigrid with full coarsening and with semicoarsening in the ξ and η directions. Residual histories are shown in Fig. 10. The results show that semicoarsening has the best convergence rate, with 56% savings in CPU time over the single grid-solution, whereas full coarsening saves 28.6% CPU time of the single-grid solution.

Comparisons were made between the calculated results and the experimental data at 10-deg angle of attack.[12] Figure 11 shows the static pressure distributions along the prolate spheroid at different circular locations around the body. Figures 12a–12c show the u-component velocity profiles at sections of X/L = 0.4, 0.6, and 0.772, where r is the normal distance from the surface. These sections were chosen for comparison because the primary separation is not yet developed at X/L = 0.4, is incipient at X/L = 0.6, and is well developed at X/L = 0.772 according to the experiment.[12] It should be remarked that the measured u velocity is in the local-freestream direction, whereas the computed u velocity is in the axial direction of the body. However, such a difference is not significant since the flow angle of attack is not large (10 deg). Computational results show good agreement with the experiments at most locations.

V. Conclusions

A nonlinear multigrid algorithm FAS for solving the three-dimensional incompressible Navier–Stokes equations with a high-resolution implicit scheme has been presented. Two methods for constructing the coarse grid operator, the GCA and the DCA, have been investigated and incorporated into the multigrid scheme. An implicit correction smoothing technique that demonstrated the capability of increasing the extent of the stability of the multigrid scheme by allowing a larger CFL number has been introduced in this work.

Solutions for turbulent flows at different high-Reynolds numbers are obtained using the current multigrid algorithm, including the flow about the SUBOFF bare hull at $Re = 1.2 \times 10^9$. All calculations were carried out on a single processor workstation. Computational results show rather favorable agreement with experimental data. The current method is robust in handling very small grid spacings and high aspect ratio grid cells for the computation of extremely high-Reynolds number turbulent flows without wall functions. The convergence of the current multigrid method is 2–3 times faster than that of the single grid, based on CPU times.

Acknowledgment

This research was supported by the Office of Naval Research (ONR) under the Grant N00014-92-J-1060 with James A. Fein as the technical monitor. This support is gratefully acknowledged.

References

[1]Marconi, F., Siclari, M., Carpenter, G., and Chow, R., "Comparisons of TLNS3D Computations with Test Data for a Transport Wing/Simple Body Configuration," AIAA Paper 94-2237, June 1994.

[2]Sheng, C., Taylor, L. K., and Whitfield, D. L., "Multiblock Multigrid Solutions of Three-Dimensional Incompressible Turbulent Flows About Appended Submarine Configurations," AIAA Paper 95-0203, Jan. 1995.

[3]Brandt, A., "Multigrid Techniques: 1984 Guide with Applications to Fluid Dynamics," *Lecture Notes for Computational Fluid Dynamics*, Lecture Series, von Kármán Inst. for Fluid Dynamics, Rhôde-Saint-Genese, Belgium, March 1984.

[4]Jameson, A., "Solution of the Euler Equations for Two Dimensional Transonic Flow by a Multigrid Method," *Applied Mathematical Computations*, Vol. 13, 1983, pp. 327–355.

[5]Anderson, W. K., Thomas, J. L., and Whitfield, D. L., "Multigrid Acceleration of the Flux Split Euler Equations," AIAA Paper 86-0274, Jan. 1986.

[6]Hemker, P. W., and Spekreijse, S. P., "Multiple Grid and Osher's Scheme for the Efficient Solution of the Steady Euler Equations," *Applied Numerical Mathematics*, Vol. 2, 1986, pp. 475–493.

[7]Whitfield, D. L., and Taylor, L. K., "Discretized Newton-Relaxation Solution of High Resolution Flux-Difference Split Schemes," AIAA Paper 91-1539, June 1991.

[8]Chorin, A. J., "A Numerical Method for Solving Incompressible Viscous Flow Problems," *Journal of Computational Physics*, Vol. 2, 1967, pp. 12–26.

[9]Roe, P. L., "Approximate Riemann Solvers, Parameter Vectors, and Difference Schemes," *Journal of Computational Physics*, Vol. 43, May 1981, pp. 357–372.

[10]Vanden, K., and Whitfield, D. L., "Direct and Iterative Algorithms for the Three-Dimensional Euler Equations," *AIAA Journal*, Vol. 33, No. 5, 1995, pp. 851–858.

[11]Huang, T. T., Liu, H.-L., Groves, N. C., Forlini, T. J., Blanton, J. N., and Gowing, S., "Measurement of Flows Over an Axisymmetric Body with Various Appendages," 19th Symposium on Naval Hydrodynamics, Seoul, Republic of Korea, Aug. 1992.

[12]Chesnakas, C. J., Simpson, R. L., and Madden, M. M., "Three-Dimensional Velocity Measurements on a 6:1 Prolate Spheroid at 10 deg Angle of Attack," Dept. of Aerospace and Ocean Engineering, Rept. VPI-AOE-202, Virginia Polytechnic Inst. and State Univ., Blacksburg, VA, Jan. 1994.

[13]Whitfield, D. L., Janus, J. M., and Simpson, L. B., "Implicit Finite Volume High Resolution Wave-Split Scheme for Solving the Unsteady Three-Dimensional Euler and Navier–Stokes Equations on Stationary or Dynamic Grids," Engineering and Industrial Research Station, Rept. MSSU-EIRS-ASE-88-2, Mississippi State Univ., Mississippi State, MS, Feb. 1988.

[14]Osher, S., and Chakravarthy, S., "Very High Order Accurate TVD Schemes," Inst. for Computer Applications in Science and Engineering, ICASE Rept. 84-44, Sept. 1984.

[15]Taylor, L. K., and Whitfield, D. L., "Unsteady Three-Dimensional Incompressible Euler and Navier–Stokes Solver for Stationary and Dynamic Grids," AIAA Paper 91-1650, June 1991.

[16]Mulder, W. A., "Multigrid Relaxation for the Euler Equations," *Journal of Computational Physics*, Vol. 60, 1985, pp. 235–252.

[17]Rosenfeld, M., and Kwak, D., "Multigrid Acceleration of a Factional-Step Solver in Generalized Curvilinear Coordinate Systems," AIAA Paper 92-0185, Jan. 1992.

[18]Schlichting, H., *Boundary-Layer Theory*, 7th ed., McGraw–Hill, New York, 1979, pp. 635–665.